THE PUBLISHING HOUSE
OF THE ROMANIAN ACADEMY

PROCEEDINGS OF THE ROMANIAN ACADEMY, Series A,
Volume 11, Number 3/2010, pp. 245–252

PRESSURE RECOVERY IMPROVEMENT IN A CONICAL DIFFUSER WITH SWIRLING FLOW USING WATER JET INJECTION

Alin I. BOSIOC[1], Constantin TĂNASĂ[1], Sebastian MUNTEAN[2], Romeo F. SUSAN-RESIGA[1]

[1] "Politehnica" University of Timişoara, Romania
[2] Romanian Academy, Timişoara, Romania
E-mail: alin@mh.mec.upt.ro

The variable demand of the energy market forces that hydraulic turbine to work at different regimes, which includes the regimes far from and the best efficiency point. In particular, for fixed-pitch blades runners, the efficiency of the turbine rapidly deteriorates at off-design operating points. Moreover, in the discharge cone downstream the runner a precessing helical vortex (called vortex rope) is developed, with associated severe pressure fluctuations. This vortex rope produces large vibrations in the hydraulic system, breakdowns of the runner blades or leads to power swing phenomenon. A novel method to mitigate the vortex rope was introduced by Resiga et al., by injecting an axial water jet from the runner crown downstream into the draft tube cone. The experimental and numerical investigations presented in this paper clearly show that the jet injection approach significantly increases the pressure recovery in the conical diffuser with swirling flow while reducing the hydraulic losses.

Key words: Draft tube; Vortex rope; Experimental investigation; Numerical simulation; Jet control.

1. INTRODUCTION

The swirling flow configuration of the outlet of a Francis runner has a major influence on the behaviour of the flow downstream in the draft tube cone [7]. When the swirling flow exiting the runner reaches a critical state, a precessing vortex (also known as vortex rope) develops in the draft tube cone. This precessing vortex rope leads to additional hydraulic losses, decreases the pressure recovery in the discharge cone, and produces large pressure fluctuation in the whole system. An experimental investigation of pressure fluctuations in correlation with the shape of the vortex rope shows that for different regimes of the opening of the guide vane the shape of the vortex rope and rotation frequency changes with the cavitation number [4]. Ciocan et al. [3] performed in the FLINDT project a detailed experimental investigation of the draft tube flow and compared the results with numerical simulations. Their analysis shows that a 3D numerical simulation reproduces very well the pressure pulsation amplitude and the vortex frequency. Also the vortex center position, vorticity and the velocity field measured with the PIV show a good agreement and validate the phenomenology of the vortex rope in numerical simulations.

As a consequence of the behaviour of the swirling flow with vortex rope, Casanova [2] presents an analysis of draft tube connecting bolts of a Francis type hydroelectric power plant. It was observed that the fracture of the bolts is frequent when the runner operates far from the best efficiency point, when the pressure fluctuation is higher than in other cases when the turbine operates close to normal conditions.

In order to eliminate or to mitigate the instabilities from the draft tube cone different techniques have been implemented in hydraulic turbines: stabilizer fins, runner cones or aerators mounted at the inlet of the cone [11]. Although these methods lead to some improvements in reducing the pressure fluctuations within certain narrow operating range, for other operating regimes they are not effective or even increase the unwanted effects. Moreover, the hydraulic losses in the draft tube are at best kept at the same level, if not increased.

Resiga et al. [6] propose a novel simple and robust method to mitigate the vortex rope: a water jet is injected from the crown of the runner, along the discharge cone axis. This technique was tested on experimentally on a test rig developed at the Hydraulic Machines Laboratory from the "Politehnica" University of Timisoara, with a test section that mimics the swirling from in a real Francis turbine.

This paper presents experimental investigations and two-dimensional axisymmetric simulations of the swirling flow in a conical diffuser in order to assess quantitatively the benefits of the jet injection on increasing the kinetic-to-static head conversion as well as on decreasing the hydraulic losses. Section 2 introduces the experimental test rig, and Section 3 describes the experimental equipment and measuring procedures. The numerical simulation approach is detailed in Section 4, where we present the computational domain, the mathematical model considered for turbulent axisymmetric swirling flows, as well as the boundary conditions that complete the problem formulation. Section 5 is devoted to numerical and experimental results, with a detailed discussion aimed at elucidating the physics of our flow control technique. The paper conclusions are summarized in Section 6.

2. EXPERIMENTAL TEST RIG

The experimental test rig was designed to investigate the decelerated swirling flow with vortex rope in a conical diffuser and also to investigate the new flow control method with axial water jet injection. The test rig has two circuits: the main circuit which is used to generate the swirling flow and the auxiliary circuit which is used to supply with water the jet. The swirl apparatus, Fig. 1, is an original design which reproduces the actual swirling flow encountered in real Francis turbines operated at partial discharge [1].

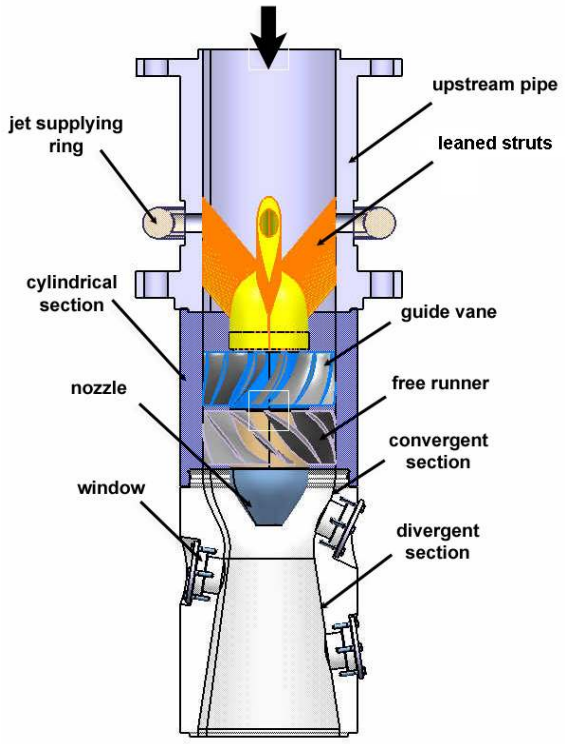

Fig. 1 – The swirl apparatus with test section from plexiglass and the swirl generator.

Instead of using a hydraulic turbine model for the experimental investigations we have designed a swirl apparatus. The convergent-divergent hydraulic passage was designed using classical wind tunnel considerations in order to achieve a uniform acceleration of the flow up to the throat, followed by a conical diffuser similar to the discharge cone of a real turbine [1]. Upstream the throat we have a swirl generator which uses two blade rows. The upstream non-rotating blades (guide vanes) produce a free-vortex rotating component, while keeping the axial velocity practically constant. However, in real turbines operated at part load there is a velocity deficit (for both axial and circumferential components) near the hub, with a corresponding excess near the shroud, for the swirling flow exiting the runner. As a result, a second row of rotating blades (free runner) is used to create a specific energy deficit near the hub with a corresponding excess near the shroud. The runner spins at the runaway speed, acting as a turbine near the hub and as a pump near the shroud, with vanishing overall torque. This swirl generator ends with a convergent section leading just downstream the throat to a swirling flow configuration similar to the one downstream a Francis runner operated at 70% the best efficiency discharge [3]. As a result, decelerating this swirling flow further downstream into the conical diffuser generates the precessing vortex rope with associated unsteady pressure field. The hub of the swirl generator is supported by four streamlined struts, which also allow the supply with water of the control jet issued through the nozzle at the end on the hub. After the conical diffuser we have a cylindrical pipe which discharges into the main reservoir. This simplified diffuser retains only the discharge cone from the real elbow draft tubes used in hydraulic turbines because the kinetic-to-static head conversion takes place mostly in this part of the turbine hydraulic passage.

The free runner speed has been measured for variable flow rate. We conclude that a linear fit accurately correlates the runner speed and the overall discharge in the main circuit of the test rig. This experimental result also confirms the performance of the water lubricated radial and axial bearings of the runner.

3. EXPERIMENTAL INVESTIGATIONS

Two kinds of measurements were performed on the swirl apparatus: the velocity measurements with Laser Doppler Velocimetry in order to validate the inlet velocity profiles used for numerical simulations and pressure measurements in order to assess the pressure recovery coefficient.

The LDV measurements were performed on an optical window mounted in the convergent part of the test section, where the swirl generated by the free runner is checked. The system consists in an argon-ion source with 300 mW power and optical fiber that guides the beams to the flow. The main characteristics of the optical systems are: focal length of the probe 159.6 mm; beam diameter 2.2 mm and the beam spacing 39.2 mm. A 3D traversing system is installed for probe positioning within 0.01 mm accuracy on each axis. On the measured axis from convergent part the measurements were made with a step size of 1 mm and in each point are measured 10000 samples or 30 seconds. Fig. 3 presents the LDV system mounted on the test rig (up) and the location of survey axis for convergent part of the test section (down).

The time averaged velocity was calculated with equation:

$$\bar{u} = \sum_{i=0}^{N-1} \frac{1}{N} \cdot u_i \,, \tag{1}$$

where N is number of samples, in our case 10,000 samples, and u_i the velocity for each sample.

The analysed data are presented in dimensionless form, using the following reference values: the minimum radius of the test section R_{throat}=50 mm and the mean velocity at the throat is the discharge velocity corresponding to the discharge Q :

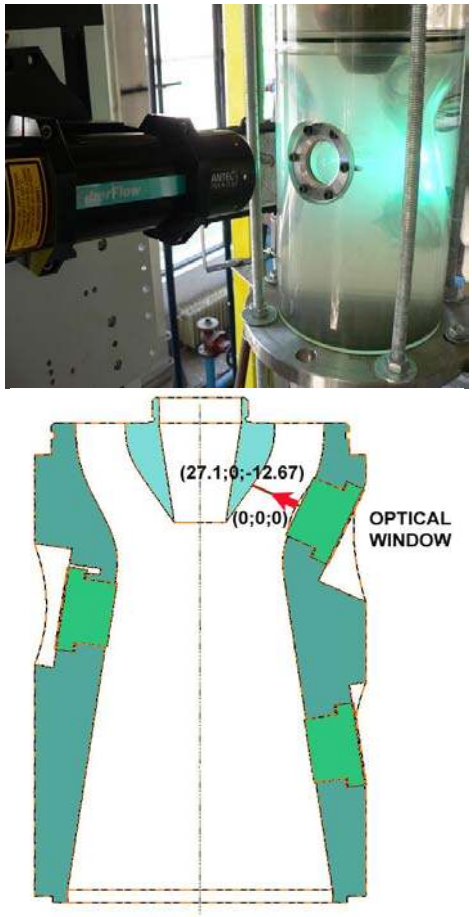

Fig. 2 – LDV system (up) and the survey axis for the convergent part of the test section (down).

$$v_{\text{throat}} = \frac{Q_{funct} + Q_{jet}}{\pi \cdot R_{\text{throat}}^2}, \tag{2}$$

where Q_{funct} is the main flow discharge and Q_{jet} is jet discharge

The plotted velocity profiles for meridian and circumferential velocity have points obtained from experimental investigation at overall discharge values of 0.03 m^3/s and 0.025 m^3/s in dimensionless values and the variation of Random Mean Square Velocity (u_{RMS}) for each point also in dimensionless values. The variation of RMS was calculated with formula:

$$u_{\text{RMS}} = \sqrt{\sum_{i=0}^{N-1} \frac{1}{N} \cdot \left(u_i - \bar{u}\right)^2} \,. \tag{3}$$

Measured meridian and circumferential velocity profiles along the survey axis from Fig. 2 are shown in Fig. 5, with error bars corresponding to the RMS values for each point. The wall static pressure is measured with eight unsteady pressure transducers mounted on the conical diffuser wall. The pressure transducers are installed in pairs, the first one corresponding to the throat, the second one at 50 mm downstream, and the next two pairs with 50 mm spacing further downstream in the conical diffuser. A picture with the pressure transducers already flash mounted on the test section is presented in Fig. 3 (up) and the name for each level in presented in Fig. 3 (down). In order to obtain reliable pressure data we measure 100 sets for each discharge value. Each set is acquired using a Lab View program, and corresponds to an acquisition time of 32 seconds at a sampling rate of 256 samples/second, resulting in 8,192 samples of unsteady pressure. The capacitive pressure transducers have an accuracy of 0.13% within a range of ±1 bar relative pressure. When the water is at

rest, all pressure transducers are aligned with respect to the static head. For the investigations reported in this paper we are interested in the time-averaged pressure values, in order to assess the wall pressure recovery for the conical diffuser without and with control jet. The dimensionless wall pressure recovery coefficient, c_p, defined as:

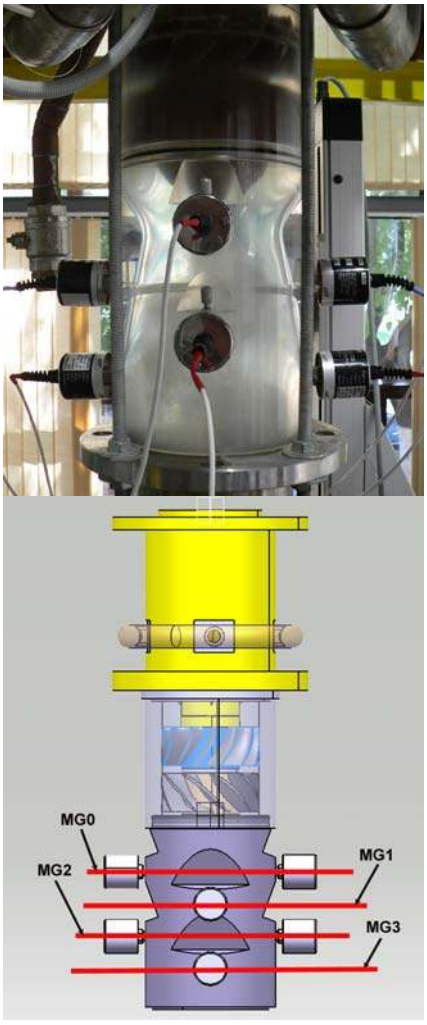

Fig. 3 – Test section with pressure transducers flash labels for each level.

$$c_p = \frac{\overline{p} - \overline{p}_{\text{throat}}}{\left(\rho \cdot v_{\text{throat}}^2\right)/2}, \tag{4}$$

where $\overline{p}$ is the time averaged value of the wall pressure, with the corresponding value at the throat $\overline{p}_{\text{throat}}$, and v_{throat} defined in Eq. (2). Experimental investigations were performed at discharge values of 30 l/s and 35 l/s. All graphs of pressure recovery coefficient contain the variation of the RMS which was calculated with formula:

$$p_{\text{RMS}} = \sqrt{\sum_{i=1}^{N_s} \frac{1}{N_s}\left(p_i - \overline{p}\right)^2}, \tag{5}$$

where N_s is number of acquired samples for each set, in our case N_s= 8,192 samples, p_i is the measured pressure for each sample. Of course, p_{RMS} is also made dimensionless with the kinetic term $\left(\rho \cdot v_{\text{throat}}^2\right)/2$.

4. NUMERICAL SIMULATIONS

The above experimental investigations offer only a limited amount of data. As a result, in order to understand the complex physics of the decelerated swirling flow we perform numerical simulations as well. As mentioned before, in the present paper we focus on the time-averaged flow field. Therefore, we consider a simplified flow model corresponding to the axisymmetric turbulent swirling flow downstream the free runner of the swirl apparatus. The 2D axisymmetrical domain for numerical simulation is presented in the Fig. 5. The annular inlet section is considered just downstream the runner blades. We then have a convergent section up to the hydraulic passage throat, and a conical diffuser ending with a discharge cylindrical pipe.

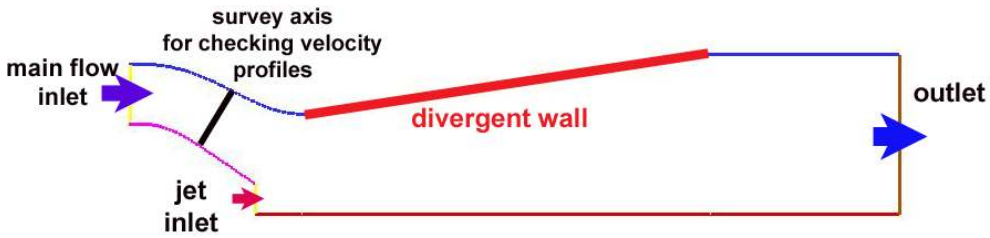

Fig. 4 – Two-dimensional computational domain in a meridian half-plane.

In the convergent section we have the survey axis where meridian and circumferential velocity profiles are validated against LDV measured ones. First, the swirl generator was analyzed numerically, using a three-dimensional turbulent flow computation. Separate sub domains were considered for the ogive with struts,

non-rotating blades, and the free runner. The mixing interface technique was employed to transfer the outlet velocity and turbulence quantities profiles from one sub-domain to the next one in the flow direction. For numerical simulation both the 3D domain for the swirl generator and 2D domain for the test section is use an unsteady SST k-ω turbulence model. The major ways in which the SST model differs from the standard model are as follows: gradual change from the standard *k-ω* model in the inner region of the boundary layer to a high Reynolds number version of the *k-ε* model in the outer part of the boundary layer and modified turbulent viscosity formulation to account for the transport effects of the principal turbulent shear stress. From the 3D domain of the free runner we impose the velocity profiles in 2D domain. Since the flow in the conical diffuser is three-dimensional and unsteady due to the development of the precessing vortex rope, one may question the relevance of an axisymmetric flow simulation. This issue was examined by Resiga et al. [9], and we concluded that the axisymmetric flow model accurately describe the circumferentially averaged three-dimensional flow field. For the 2D simulation the governing equations for axisymmetric swirling flows and incompressible fluids were obtained by writing both the continuity and the momentum equations in cylindrical coordinates, then discarding the derivates with respect to the circumferential coordinate. More detailed analysis of the equations is presented in Resiga et al. [10].

The continuity equation is:

$$\nabla \cdot \mathbf{V} = \frac{\partial V_z}{\partial z} + \frac{\partial V_r}{\partial r} + \frac{V_r}{r} = 0 \cdot \tag{6}$$

The axial momentum equation is:

$$\frac{\partial V_z}{\partial t} + \frac{1}{r}\frac{\partial}{\partial z}(rV_zV_z) + \frac{1}{r}\frac{\partial}{\partial r}(rV_rV_z) = -\frac{1}{\rho}\frac{\partial p}{\partial z} + \frac{1}{r}\frac{\partial}{\partial z}\left[r\frac{\mu+\mu_T}{\rho}2\frac{\partial V_z}{\partial z}\right] + \frac{1}{r}\frac{\partial}{\partial r}\left[r\frac{\mu+\mu_T}{\rho}\left(\frac{\partial V_z}{\partial r}+\frac{\partial V_r}{\partial z}\right)\right]. \tag{7}$$

The radial momentum equation is:

$$\begin{aligned}&\frac{\partial V_r}{\partial t} + \frac{1}{r}\frac{\partial}{\partial z}(rV_zV_r) + \frac{1}{r}\frac{\partial}{\partial r}(rV_rV_r) = \\ &= -\frac{1}{\rho}\frac{\partial p}{\partial r} + \frac{V_\theta^2}{r} + \frac{1}{r}\frac{\partial}{\partial z}\left[r\frac{\mu+\mu_T}{\rho}\left(\frac{\partial V_r}{\partial z}+\frac{\partial V_z}{\partial r}\right)\right] + \frac{1}{r}\frac{\partial}{\partial r}\left[r\frac{\mu+\mu_T}{\rho}2\frac{\partial V_r}{\partial r}\right] - 2\frac{\mu+\mu_T}{\rho}\frac{V_r}{r^2}.\end{aligned} \tag{8}$$

The circumferential momentum equation is:

$$\frac{\partial V_\theta}{\partial t} + \frac{1}{r}\frac{\partial}{\partial z}(rV_zV_\theta) + \frac{1}{r}\frac{\partial}{\partial r}(rV_rV_\theta) = -\frac{V_rV_\theta}{r} + \frac{1}{r}\frac{\partial}{\partial z}\left[r\frac{\mu+\mu_T}{\rho}\frac{\partial V_\theta}{\partial z}\right] + \frac{1}{r^2}\frac{\partial}{\partial r}\left[r^3\frac{\mu+\mu_T}{\rho}\frac{\partial}{\partial r}\left(\frac{V_\theta}{r}\right)\right]. \tag{9}$$

The effective dynamic viscosity is calculated as the sum at the so called turbulent viscosity μ_T and the molecular viscosity μ. The axisymetric swirling flow model which is implemented in the FLUENT 6.3 code is used with the turbulence model which was described above.

At the outlet of the computational domain a radial equilibrium condition is used which involves the radial pressure gradient with the circumferential velocity:

$$\frac{\partial p}{\partial r} = \frac{\rho V_\theta^2}{r}. \tag{10}$$

5. EXPERIMENTAL AND NUMERICAL RESULTS

Once the numerical solution for the axisymmetric turbulent swirling flow is obtained, we first check the accuracy of the inlet velocity profiles. In doing so, we compare the computed meridian and circumferential velocity profiles with the LDV measurements on the survey axis located in the convergent section. The results are shown in Fig. 5, where a very good agreement between computations and measurements is observed, thus validating the overall accuracy of the 3D flow computation in the bladed region of the swirl generator. Moreover, since the velocity survey axis is located in the convergent part of the swirl apparatus, upstream the jet nozzle, the velocity profiles are not altered by the jet injection. Once the velocity profiles in the convergent part validated, we focus on the wall pressure recovery coefficient for two cases: the case of the swirling flow without jet control and with jet injection. For the first case in numerical simulation was calculated the wall pressure recovery coefficient in three variants function of the domain meshing. From the comparison between the three models with 30,000 cells, 50,000 cells and 120,000 cells,

the wall pressure recovery coefficient it has the same value, so we decided that the fallowed simulations to be with minimum values of cells in order to have a quick result in a short time.

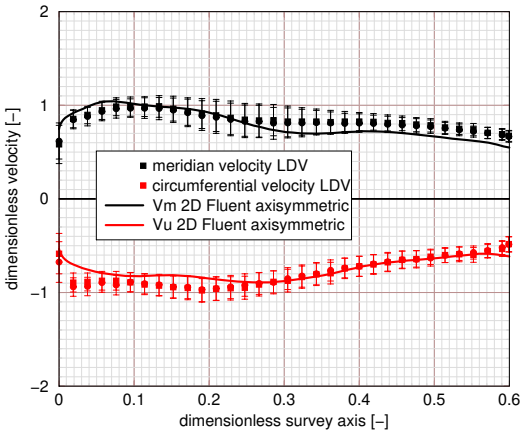

Fig. 5 – Comparison of velocity profiles between experimental investigation and numerical simulation in the convergent part of the test section.

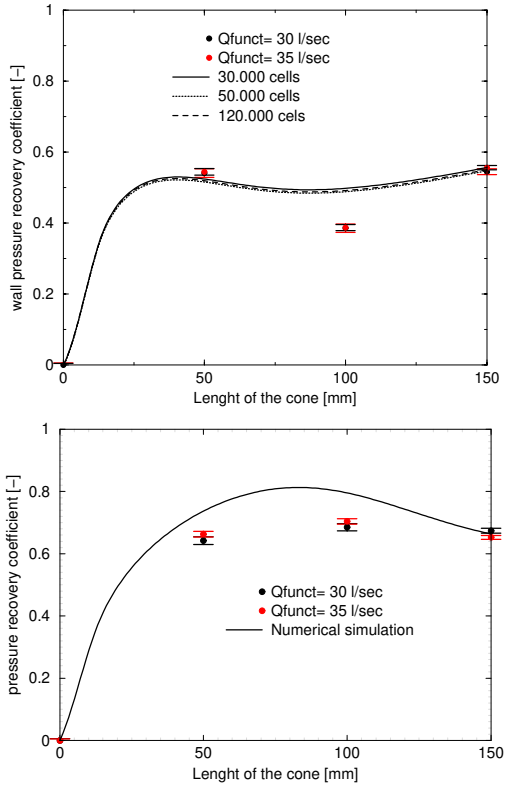

Fig. 6 – Wall pressure recovery coefficient for the case without jet control (up) and with jet control (down).

Fig. 6 (up) shows the wall pressure coefficient computed from the axisymmetric turbulent swirling flow simulation (curves for three levels of grid refinement) and the measured values at the positions indicated in Section 3. We see that the wall pressure recovery reaches a value of approximately 0.55 when the decelerated swirling flow has a precessing vortex rope. Once again, in this paper we examine only the time averaged flow field, in order to assess the influence of our flow control approach on the overall diffuser efficiency. The computational results in Fig. 6 (up) agree well with the measured pressure recovery coefficient, with an overestimation of the experimental value obtained in the middle of the conical diffuser, at 100 mm distance from the throat. We explain this difference by the large amplitude of the pressure fluctuations in this region due to the precessing vortex rope.

We gradually increase the jet discharge in order to mitigate the vortex rope, and conclude that a 10% jet discharge with respect to the main flow discharge is required to stabilize the flow for our experiment. We can observe from Fig. 6 (down), that when we inject the water jet along the axis the wall pressure recovery coefficient increases up to approximately 0.72, this is 30% larger than the previous value of 0.55 without jet. This is an important improvement in the diffuser performance, which for real turbines will lead to a corresponding increase of the overall performance. The numerical results agree reasonably well with the measured values of the wall pressure recovery coefficient. From the above results it is rather difficult to understand the correlation between the jet injection along the diffuser axis and the increase in the pressure recovery coefficient on the diffuser wall. This is why we focus now on the computed flow field to understand and explain this correlation. We recall the qualitative vortex rope model proposed by Nishi et al. [5]. As shown in Fig. 7, the vortex rope evolves from the instability of a vortex sheet which rolls-up as a helical vortex (spiral vortex core) around a central stalled region. This central region is highly oscillating due to the helical vortex precession, but on average it has a vanishing velocity as we have shown in [10]. This feature specific to decelerated swirling flows is correctly captured by the axisymmetric swirling flow model, as shown in Fig. 9, upper picture. Because of the large swirl level, the flow is strongly decelerated near the axis leading to a stagnant region. The main flow is confined in an annular region close to the wall, with a rather modest deceleration. This is why the wall pressure recovery has lower values in this case, as shown in Fig. 6 (up). When the water jet is injected, the central stagnant region is pushed downstream, out of the conical diffuser, Fig. 8 lower picture, and the main flow decelerates by occupying the whole cross section of the conical diffuser. The jet injection mitigates the stagnant region and accelerates the main flow near the axis as shown by the streamline pattern, thus significantly improving the pressure recovery in the conical diffuser.

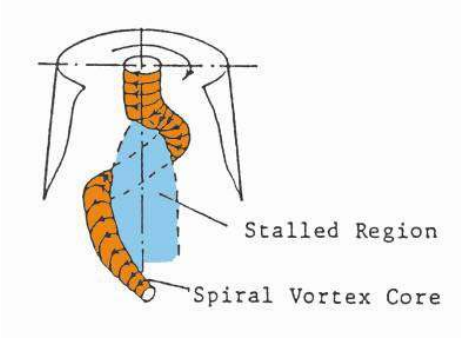

Fig. 7 – Stagnant region model for swirling flow with precessing vortex rope, Nishi et al. [9].

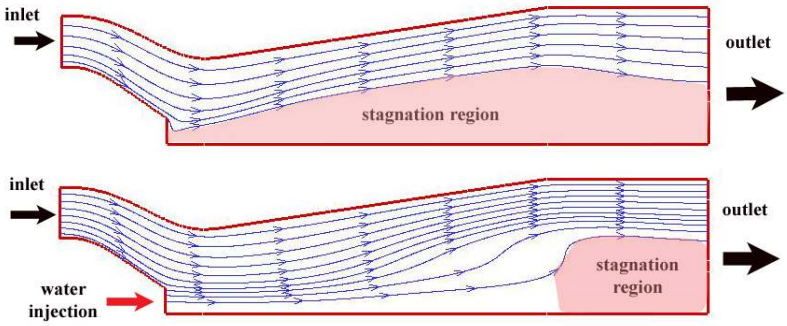

Fig. 8 – Streamlines for swirling flow without (up) and with water jet control (down).

The above qualitative analysis based on the streamline pattern is further complemented by a quantitative assessment of the evolution of the static, kinetic and total head in the diffuser. We first define for an arbitrary cross section (normal to the symmetry axis) the following quantities:

$$\Pi(x) = \int_{S(x)} p(x,r)\mathbf{V}\cdot\mathbf{n}\,\mathrm{d}S \quad [\mathrm{W}], \tag{11}$$

$$K(x) = \int_{S(x)} \frac{\rho V^2(x,r)}{2}\mathbf{V}\cdot\mathbf{n}\,\mathrm{d}S \quad [\mathrm{W}], \tag{12}$$

$$E(x) = \Pi(x) + K(x) \quad [\mathrm{W}]. \tag{13}$$

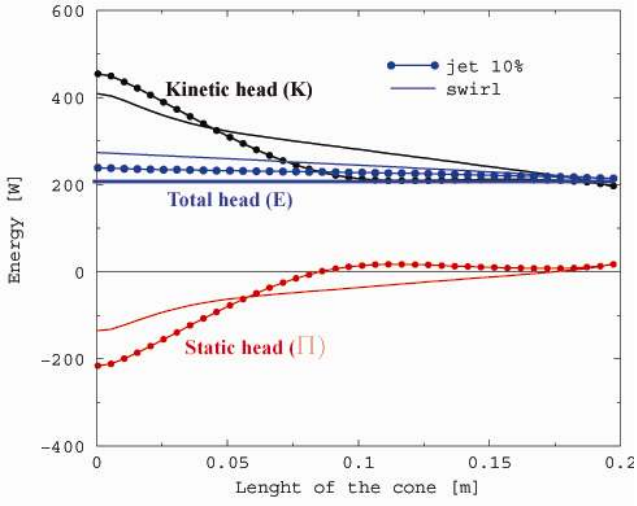

Fig. 9 – The fluxes of kinetic head K, total head E and static head Π, without and with jet control.

Then, we examine the evolution of these integral quantities from the throat up to the exit of the cone, as shown in Fig. 9. As expected for a diffuser, as the flow evolves downstream the static head increases with a corresponding decrease in kinetic head due to the flow deceleration. The total head is a continuously decreasing curve due to the hydraulic losses. As we can see from Fig. 9, the kinetic-to-static head conversion is significantly improved by the jet injection, within the upstream part of the conical diffuser. This result is particularly important for hydraulic turbines, where short discharge cones are used for modern draft tubes. We conclude that the jet injection has the potential of improving the pressure recovery in discharge cones of real turbines over a wide operating range. This is a particular requirement for modern hydraulic turbines which are operated within a large range, far from the best efficiency point. The slope of the total head decrease is smaller when the jet is injected in comparison with the initial situation when the vortex rope is present in the cone. This means that the hydraulic losses are reduced in our case to practically half the initial value by the jet injection. As a result, the overall efficiency hill chart of the turbine is flattened as required for both new turbines and refurbished ones.

6. CONCLUSIONS

We investigate in this paper the decelerated swirling flow in conical diffuser, with a configuration that mimics the flow in the discharge cone of hydraulic turbines operated at partial discharge. In particular, we examine a novel flow control technique which uses a jet injection along the axis in order to improve the pressure recovery while reducing the hydraulic losses. The wall pressure recovery measurements on the conical diffuser show that the jet injection leads to a 30% improvement. This is extremely useful for

hydraulic turbines when operated far from the best efficiency point, leading to a significant overall increase in the performance. In order to elucidate the correlation between the jet injection along the axis and the increase in pressure recovery we perform numerical simulations of the decelerated turbulent swirling flow using an axisymmetric flow model. The inlet boundary conditions for our numerical simulation are validated with very good accuracy against Laser Doppler Velocimetry measurements of the meridian and circumferential velocity profiles in the upstream part of the test section. The analysis of the streamline pattern in a meridian half plane shows that the initial swirling flow develops a large central quasi-stagnant region. As result, the main flow is confined in an annular section close to the cone wall, with modest deceleration and rather small pressure recovery. This effect deteriorates the overall performance of the hydraulic turbines operated at partial discharge. However, when the jet is injected the main flow is accelerated near the axis and occupies the whole cross-section of the cone. As a result, the jet significantly increases the cross section of the main flow, leading to an overall deceleration and the corresponding significant increase in pressure recovery.

The qualitative analysis of the streamline pattern is complemented with a quantitative assessment of the evolution of the static, kinetic and total head within the cone. It is shown that when we inject the control jet, the kinetic-to-static head conversion increases by almost 50%, while reducing to a half the overall hydraulic losses. This result clearly shows the potential of our flow control method to flatten the hillchart of Francis hydraulic turbines when operated at off-design regimes, the efficiency maintaining at high values. Moreover, the increase in the conical diffuser performance takes place in the upstream half of the cone, showing that compact discharge cones can be successfully used for modern draft tubes, without diminishing the pressure recovery, if the jet injection is implemented.

The present paper was focused on the time-averaged flow field, but the jet injection does not only improve the efficiency of the kinetic-to-static head conversion in the discharge cone of hydraulic turbines but also successfully mitigated the pressure fluctuations associated with the precessing vortex rope.

ACKNOWLEDGEMENTS

The authors would like to thanks for support to the CNCSIS PCE 799 project.

REFERENCES

1. BOSIOC, A.I., SUSAN-RESIGA, R.F., MUNTEAN, S., *Design and Manufacturing of a Convergent-Divergent Test Section for Swirling Flow Apparatus*, communicated at the 4th German-Romanian Workshop on Turbomachinery, Stuttgart, 2008.
2. CASANOVA, F., *Failure analysis of the draft tube connecting bolts of a Francis-type hydroelectric power plant*, Engineering Failure Analysis, **16**, pp. 2202–2208, 2009.
3. CIOCAN, G.D., ILIESCU, M.S., VU, T.C., NENNEMANN, B., AVELLAN, F., *Experimental Study and Numerical Simulation of the FLINDT Draft Tube Rotating Vortex,* Journal of Fluids Engineering, **129**, pp. 146–158, 2007.
4. KIRSCHNER, O., RUPRECHT, A., GODE, E., *Experimental investigation of pressure pulsation in a simplified draft tube*, Proceedings of the 3rd IAHR International Meeting of the Workgroup on Cavitation and Dynamic Problems in Hydraulic Machinery and Systems, Brno, Czech Republic, 2009 pp. 55–65.
5. NISHI, M., MATSUNAGA, S., KUBOTA, T., SENOO, Y., *Flow Regimes in an Elbow-Type Draft Tube*, IAHR Symposium, Operating Problems of Pump Stations and Power Plants, 1987.
6. SUSAN-RESIGA, R.F., VU. T.C., MUNTEAN, S., CIOCAN G.D., NENNEMANN, B., *Jet Control of the Draft Tube in Francis Turbines at Partial Discharge*, Proceedings of the 23rd IAHR Symposium on Hydraulic Machinery and Systems, Yokohama, Japan, 2006 p. 192.
7. SUSAN-RESIGA, R.F., CIOCAN, G.D., ANTON, I., AVELLAN, F., *Analysis of the swirling flow downstream a Francis turbine runner*, Journal of Fluids Engineering, **128**, pp. 177–189, 2006.
8. SUSAN-RESIGA, R.F., MUNTEAN, S., *Decelerated swirling flow control in the discharge cone of Francis turbines*, The 4th International Symposium on Fluid Machinery and Fluid Engineering, Beijing, China, 2008 p. 89–96.
9. SUSAN-RESIGA, R.F., MUNTEAN, S., TANASA, C., BOSIOC, A., Three-Dimensional versus Two-Dimensional Axisymmetric Analysis for decelerated Swirling Flows, Proceedings of the 13th International Conference on Fluid Flow, Budapest, Hungary, pp. 862–869, 2009.
10. SUSAN-RESIGA, R.F., MUNTEAN S., STEIN, P., AVELLAN, F., *Axisymmetric Swirling Flow Simulation of the Draft Tube Vortex in Francis Turbines at Partial Discharge*, IJFMS, **2**, *4*, pp. 295–302, 2009.
11. THICKE, R.H., *Practical solutions for draft tube instability*, Water Power & Dam Construction, pp. 31–37, 1981.

Received February 5, 2010